

A Chimeric Antibody against ACKR3/CXCR7 in Combination with TMZ Activates Immune Responses and Extends Survival in Mouse GBM Models

Nicole Salazar,^{1,2} Jeffrey C. Carlson,² Kexin Huang,³ Yayue Zheng,² Cecilia Oderup,^{1,2} Julia Gross,² Andrew D. Jang,² Thomas M. Burke,² Susanna Lewén,² Alexander Scholz,^{1,2} Serina Huang,² Leona Nease,² Jon Kosek,² Michel Mittelbronn,^{4,5,6,7,8} Eugene C. Butcher,^{1,2} Hua Tu,³ and Brian A. Zabel²

¹Department of Pathology, Stanford University School of Medicine, Stanford, CA, USA; ²Palo Alto Veterans Institute for Research (PAVIR), Veterans Affairs Palo Alto Health Care System (VAPAHCS), Palo Alto, CA, USA; ³LakePharma Inc., Belmont, CA, USA; ⁴Institute of Neurology, Edinger Institute, Frankfurt, Germany; ⁵Luxembourg Centre of Neuropathology (LCNP), Luxembourg City, Luxembourg; ⁶Department of Pathology, Laboratoire National de Santé, Dudelange, Luxembourg; ⁷Luxembourg Centre for Systems Biomedicine (LCSB), University of Luxembourg, Esch-sur-Alzette, Luxembourg; ⁸NORLUX Neuro-Oncology Laboratory, Department of Oncology, Luxembourg Institute of Health, Luxembourg City, Luxembourg

Glioblastoma (GBM) is the least treatable type of brain tumor, afflicting over 15,000 people per year in the United States. Patients have a median survival of 16 months, and over 95% die within 5 years. The chemokine receptor ACKR3 is selectively expressed on both GBM cells and tumor-associated blood vessels. High tumor expression of ACKR3 correlates with poor prognosis and potential treatment resistance, making it an attractive therapeutic target. We engineered a single chain FV-human FC-immunoglobulin G1 (IgG₁) antibody, X7Ab, to target ACKR3 in human and mouse GBM cells. We used hydrodynamic gene transfer to overexpress the antibody, with efficacy *in vivo*. X7Ab kills GBM tumor cells and ACKR3-expressing vascular endothelial cells by engaging the cytotoxic activity of natural killer (NK) cells and complement and the phagocytic activity of macrophages. Combining X7Ab with TMZ allows the TMZ dosage to be lowered, without compromising therapeutic efficacy. Mice treated with X7Ab and in combination with TMZ showed significant tumor reduction by MRI and longer survival overall. Brain-tumor-infiltrating leukocyte analysis revealed that X7Ab enhances the activation of M1 macrophages to support anti-tumor immune response *in vivo*. Targeting ACKR3 with immunotherapeutic monoclonal antibodies (mAbs) in combination with standard of care therapies may prove effective in treating GBM.

INTRODUCTION

Glioblastoma multiforme (GBM) is the most aggressive form of brain cancer. GBM is considered incurable. With the best available care, a combination of temozolomide (TMZ) and radiotherapy (RT), the median survival for GBM is approximately 16 months, with a 5-year survival rate of 3.3%.¹ The current conventional therapy, TMZ/RT usually fails due to cancer cell resistance, and patients are next treated with Avastin, a potent anti-angiogenic antibody that also fails after approximately 5 months due to hypoxia-mediated resistance.¹

The C-X-C chemokine receptor 7 (CXCR7) ACKR3 has recently been identified across independent studies as an actionable target for treatment of GBM.^{2–6} ACKR3 is a unique target for cancer therapy due to its overexpression on both tumor cells and tumor endothelial cells.^{7,8} ACKR3 surface protein is evident on activated endothelium or tumor tissue while low to absent on the cell surface of normal adult tissues.⁹ The receptor is required for embryonic development, where it acts as a scavenger for CXCL12 to generate a gradient for proper CXCR4+ primordial germ cell migration.^{10–13}

To evaluate the potential of targeting ACKR3 in GBM, we generated a single chain anti-ACKR3 antibody (X7Ab), with a human fragment crystallizable (huFC) domain capable of mobilizing anti-tumor innate immune defenses. We assessed X7Ab for its cellular mechanism of action against GBM. We also asked whether in combination with TMZ, X7Ab could improve survival in mouse GBM models.

RESULTS

ACKR3 in Human Glioma

High ACKR3 expression significantly correlated with poor survival in patients with high-grade glioma (astrocytomas and glioblastomas, also known as grade III and IV astrocytoma, respectively)¹⁴ (Figure 1A). The overall survival in human clinical trials for GBM only (grade IV astrocytoma) did not reach statistical significance ($p < 0.05$) when divided by ACKR3/CXCR7 high versus low expression. However, at the 3- and 5-year survival time points for each study, ACKR3/CXCR7 high-expressing patients have consistently lower survival odds (Figure S1). High ACKR3 expression significantly

Received 9 September 2017; accepted 27 February 2018;
<https://doi.org/10.1016/j.ymthe.2018.02.030>

Corresponding: Brian A. Zabel, PhD, Palo Alto Veterans Institute for Research (PAVIR), Veterans Affairs Palo Alto Health Care System (VAPAHCS), m/c 154F, 3801 Miranda Ave., Palo Alto, CA 94034, USA.

E-mail: bazabel@alum.mit.edu



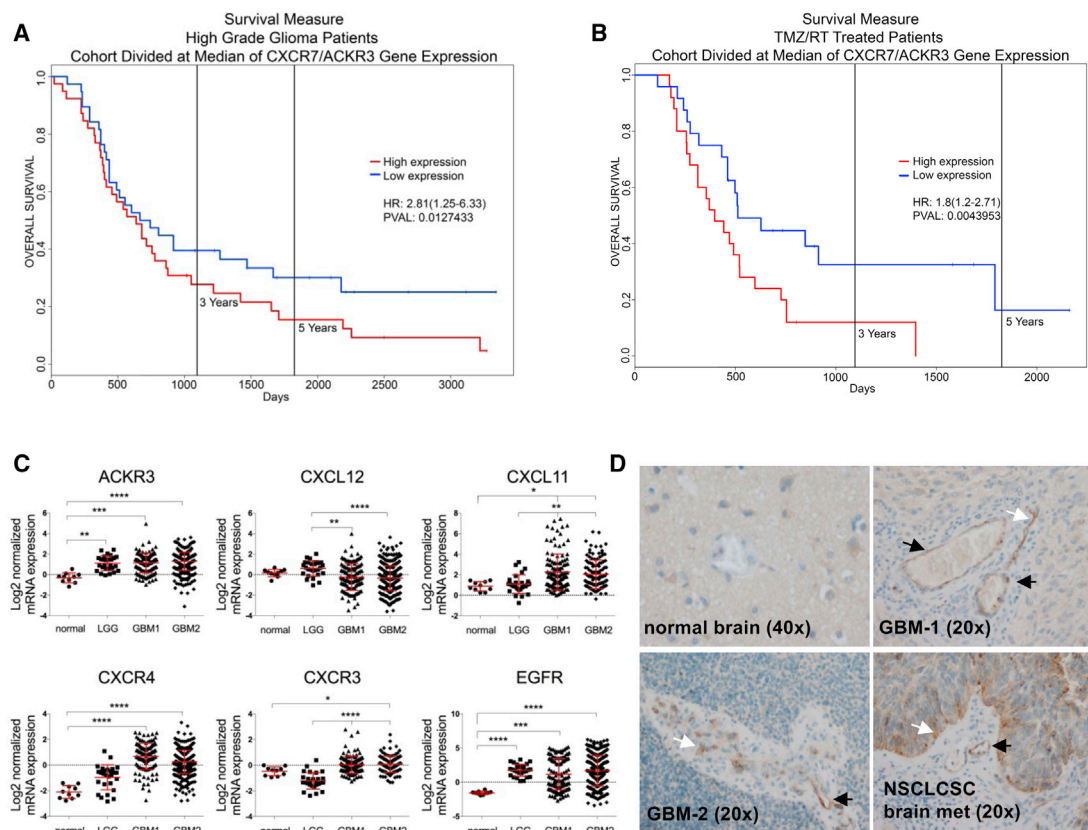


Figure 1. ACKR3 Is Upregulated in GBM and Associated with Poor Survival Outcomes

(A) mRNA microarray data (NCBI: GSE4271_U133B) from a cohort of 77 patients with high-grade glioma (astrocytomas [grade III] and glioblastomas [grade IV]), divided at the median of ACKR3 expression. Patient survival was plotted for each group (high or low relative ACKR3 expression). Hazard ratio: 2.81 (1.25–6.33), $p = 0.0127$, indicating that high ACKR3 significantly correlated with poor survival. (B) mRNA microarray data (NCBI: GSE7696) from a cohort of 49 GBM patients treated with TMZ and RT divided at the median of ACKR3 gene expression. Patient survival was plotted for each group (high or low relative ACKR3 expression). Hazard ratio: 1.8 (1.2–2.71), $p = 0.004$, indicating that high ACKR3 significantly correlated with poor survival in TMZ/RT-treated GBM patients. (C) mRNA microarray gene expression data retrieved from the TCGA database, normalized, and processed as Log₂ values were analyzed for ACKR3, CXCL12, CXCL11, CXCR4, CXCR3, and EGFR expression in a normal brain, lower grade glioma (LGG); and GBM. GBM1 indicates Agilent 1. GBM2 indicates Agilent 2 TCGA platform codes. ANOVA with post hoc Kruskal Wallis test for multiple comparisons. * $p < 0.05$; *** $p < 0.001$; **** $p < 0.0001$. (D) Brain cancer histopathology. Primary GBM tumors (2 patients), brain metastases (1 patient), and tumor-associated vessels in the CNS are ACKR3+. White arrows, ACKR3+ primary tumor cells. Black arrows, ACKR3+ tumor-associated vessels. (× magnification) indicated.

correlated with poor survival outcomes in TMZ/RT-treated GBM patients (Figure 1B). We used the TCGA database to assess ACKR3 RNA expression in normal and brain cancer tissue. ACKR3 expression was significantly elevated in lower grade glioma (LGG) and GBM compared to normal brain samples (Figure 1C). Expression of ACKR3-associated genes: endogenous ACKR3 ligands CXCL11 and CXCL12; CXCR4 (which also binds to CXCL12 and was reported to heterodimerize with ACKR3¹⁵); CXCR3, a second receptor for CXCL11; and epidermal growth factor receptor (EGFR) (which co-localizes with ACKR3 in tumor cells^{16,17}). To varying degrees, each of these ACKR3-related molecules was also upregulated in GBM (Figure 1C), consistent with reports from previous glioma studies.^{3,18,19} GBM tumor cells and tumor-associated vessels stained positive for ACKR3 protein, whereas normal brain tissue did not (Figure 1D) in CNS tissue sections from two primary GBM patients and one

non-small cell lung cancer squamous cell carcinoma (NSCLCSC) brain metastasis patient. Although the level of ACKR3 protein staining (brown) in the primary GBM samples was not as strong as that observed in the NSCLCSC metastasis sample, the level of staining was above the background level of the normal sample, indicating ACKR3 protein expression. Thus, consistent with other reports, we found that ACKR3 is selectively expressed in GBM, and elevated ACKR3 expression correlates with poor clinical outcomes.

X7Ab Binds ACKR3

We generated an anti-ACKR3 single chain antibody (X7Ab) with a human immunoglobulin G1 (IgG₁) FC sequence based on the US Food and Drug Administration (FDA)-approved Rituximab FC domain (Figure 2A). The binding affinity (dissociation constant [K_D]) of X7Ab for ACKR3 was 4.1 nM, as determined by optical

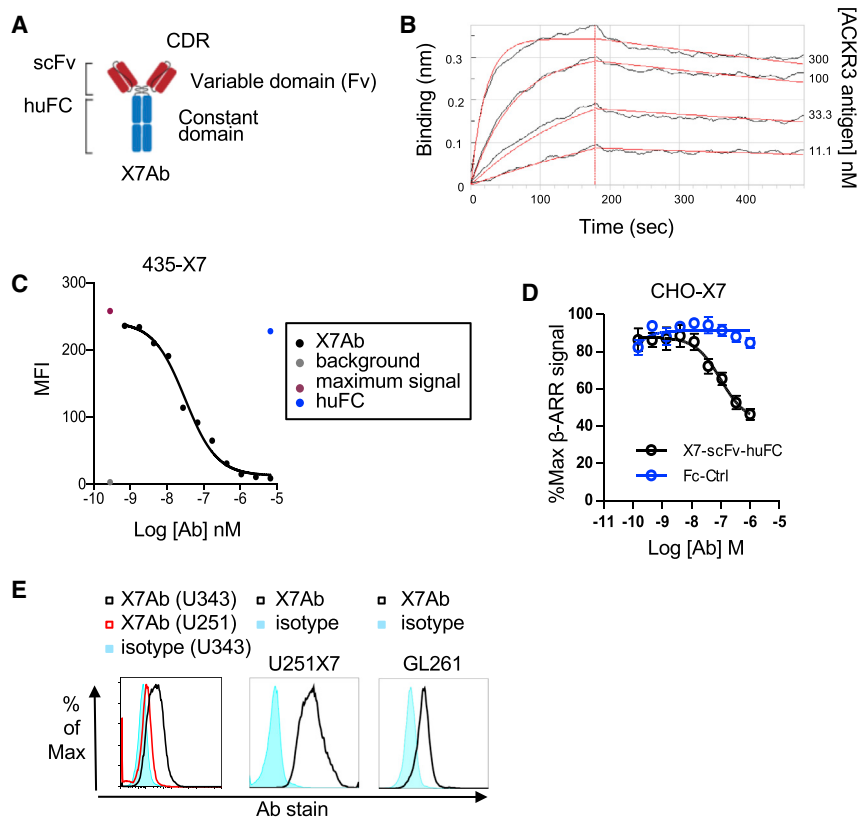


Figure 2. A High-Affinity Human-Mouse Chimeric Antibody to ACKR3

(A) Schematic of single chain FV-human FC-IgG₁ antibody specific for ACKR3 (X7Ab). (B) Binding affinity (K_D) determination for X7Ab. An Octet Qke system using anti-human FC biosensors was used to measure the kinetics of association and dissociation of X7Ab and ACKR3 by surface-based biolayer interferometry. Association with various concentrations of ACKR3 antigen (300, 100, 33.3, and 11.1 nM) was measured over 180 s, and dissociation was monitored for 300 s. Experimental data are in black and statistical fitting of curves are red. (C) Competition binding was used to determine the binding potency. Directly labeled α -ACKR3 mAb 11G8-PE was used as the tracer. 435-X7 cells were incubated with various concentrations of unlabeled X7Ab (black symbols) or 10 μ M huFC (blue symbol) as the negative control, and displacement of 11G8-PE tracer was determined by analysis of MFI by flow cytometry. No tracer (background, gray) and maximum signal (tracer only, purple symbol); IC_{50} : 30 nM. (D) X7Ab inhibits CXCL12-mediated β -arrestin2 association with ACKR3. ACKR3/ β -ARR2 CHO cells (CHOX7) were incubated with the indicated concentrations of X7Ab or FC-control and 10 nM recombinant CXCL12. For each point, the mean \pm SEM of $n = 3$ wells is shown. (E) X7Ab specifically stains ACKR3+ human cancer cells. Human GBM cell lines U251 (ACKR3 negative) and U343 (ACKR3+); human U251X7 transfectant (ACKR3+); and mouse GL261 (ACKR3+) were stained with X7Ab and analyzed by flow cytometry. Representative histograms of at least $n = 3$ experiments with similar results are shown.

biosensor interferometry (Figure 2B). The binding potency (IC_{50}) of X7Ab in inhibiting fluorescently labeled anti-ACKR3 mAb binding to ACKR3 was 30 nM, as determined by competitive binding assay and flow cytometry (Figure 2C). X7Ab inhibited CXCL12-mediated β -arrestin2 signaling (Figure 2D). X7Ab also specifically stained ACKR3+ human breast cancer cell line transfectants (435-X7) but not parental 435-WT cells (Figure S2A²⁰). X7Ab stained the human U343 glioma cell line previously shown to express endogenous ACKR3²¹ and human U251 ACKR3+ transfectants (U251X7), but not parental U251-WT glioma cells. In addition to human ACKR3, X7Ab specifically recognized mouse ACKR3 because it stained mouse ACKR3/HEK293 transfectants and E13 primitive red blood cells previously shown to express endogenous ACKR3⁷ (Figure S2B). Mouse glioma GL261 also expressed low levels of endogenous surface ACKR3 and was stained with X7Ab. Thus, we confirmed by multiple methods that X7Ab specifically binds to ACKR3 (Figure 2E).

Functional *In Vitro* Anti-tumor Activity of X7Ab

We asked if X7Ab could kill tumor cells by antibody-mediated effects, such as antibody-dependent cell cytotoxicity (ADCC), complement-dependent cytotoxicity (CDC), and antibody-dependent cellular phagocytosis (ADCP). We incubated various concentrations of X7Ab with tumor cells, and added various numbers of effector cells to cover a wide range of E:T ratios (indicated on figure legends). X7Ab triggered specific human peripheral blood mononu-

clear cell (PBMC)-driven ADCC killing of U343, U251X7, and GL261 cells (Figures 3A–3C). To determine if X7Ab can target activated endothelium known to express ACKR3, we tested human umbilical vein endothelial cells (HUVECs) treated with tumor necrosis factor alpha (TNF- α) to upregulate ACKR3.⁸ X7Ab specifically killed the ACKR3+ endothelial cells compared to FC-control via human PBMC ADCC (Figure S3), although not to a statistically significant level. Next, we assessed the killing capacity of human natural killer (NK) cell lines with CD16 (FC receptor) affinity variants because NK cells are likely the key lymphocyte subset driving ADCC *in vivo*.^{22,23} NK cell lines NK92.05 CD16-176F (lower affinity FC binding) and CD16-176V (higher affinity FC binding) effectively utilized X7Ab to kill GBM tumor targets by ADCC (Figure 3D). The X7Ab ADCC potency (EC_{50}) for the CD16-176F variant was 3.9 μ g/mL and 1.8 μ g/mL for the CD16-176V variant. The ADCC activity was specific for ACKR3 because the viability of U251-WT parent cells was unaffected by X7Ab (Figure 3E). We used the lipopolysaccharide (LPS)-activated mouse macrophage cell line RAW264.7 and the phorbol 12-myristate 13-acetate (PMA)-activated human monocytic cell line U937 as *in vitro* models of macrophages for ADCP. X7Ab also significantly enhanced the percentage of tumor cells engulfed by macrophages compared with negative controls (the ADCP effect was more pronounced with mouse macrophage effectors), and X7Ab-dependent phagocytosis required ACKR3 expression by the target (Figures 3F and 3G).

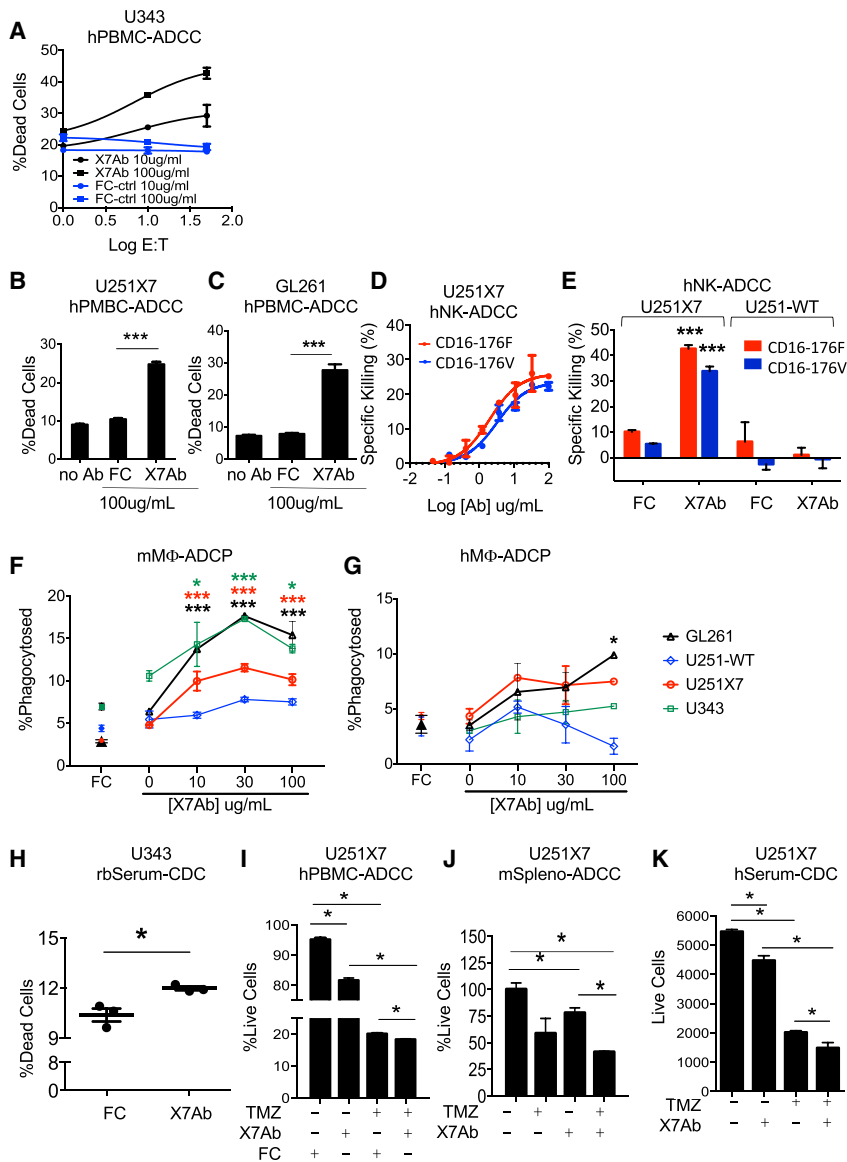


Figure 3. X7Ab-Directed Effector Killing Mechanisms

Target cells were untreated or incubated with X7Ab or FC-control (Ab concentrations as indicated) and then incubated with immune effector cells (or complement) at various E:T ratios, with target cell killing quantified by flow cytometry. (A) hPBMC X7Ab ADCC against low-expressing ACKR3+ cells U343; mean of duplicate wells \pm range. (B) hPBMC X7Ab ADCC against U251X7 and (C) GL261; E:T ratio of 30:1; mean of triplicate wells \pm SEM shown, * $p < 0.05$ by t test. (D and E) Human NK cell lines (92.05 CD16-176F and CD16-176V) mediated X7Ab ADCC against U251X7 in a dose-dependent manner (D) specifically against U251X7 and not the parent U251-WT cells, E:T 3:1, * $p < 0.05$ by t test (100 μ g/mL [Ab]) (E). (F and G) Mouse (F) and human (G) macrophage-mediated ADCC. E:T ratio of 5:1. * $p \leq 0.05$, *** $p \leq 0.001$ by two-way ANOVA Dunnett's test comparison between E+T cells alone (0 μ g/mL) and the different concentrations of antibody indicated. (H) X7Ab (100 μ g/mL) CDC against U343 with rabbit serum (25%). Mean of triplicate wells \pm SEM is shown, * $p < 0.05$ by t test. (I) Combination treatment with TMZ and X7Ab ADCC using hPBMC, E:T ratio of 100:1 (J) or mouse splenocyte (mSpleno), E:T ratio of 30:1 effectors to U251X7 targets. Tumor cells were incubated \pm TMZ (6 μ M) for 5 days and then subjected to ADCC (100 μ g/mL X7Ab or FC-control); the data were normalized to the average of the total number of viable targets in the untreated wells (set to 100% viable cell targets). Mean of triplicate wells \pm SEM is shown, * $p < 0.05$ by t test. (K) CDC of TMZ and X7Ab combination. U251X7 cells were incubated \pm TMZ (3 μ M) \pm X7Ab (30 μ g/mL) in human serum (25%). Mean of triplicate wells \pm SEM, * $p < 0.05$ by t test.

X7Ab alone had no specific effect on endogenous ACKR3-expressing U343 and GL261 cells or ACKR3-U251 cell viability *in vitro*, with a minor cytotoxic effect at the highest level of treatment on ACKR3+ U251X7 cells (Figure S4), leading us to conclude that X7Ab primarily requires a FC-dependent mechanism to engage anti-tumor immune defenses. X7Ab also induced a weak but significant CDC response in U343 cells compared with FC-control (Figure 3H).

Combination Strategy

X7Ab-mediated ADCC combined with TMZ induced significantly more GBM cell death than either agent used alone (Figures 3I and 3J). This was true using human PBMC effectors (Figure 3I) or SCID splenocyte effectors (Figure 3J). As with ADCC, X7Ab-medi-

ated CDC combined with TMZ induced significantly more GBM cell death than either agent used singly (Figure 3K).

HDT to Overexpress X7Ab Protein *In Vivo*

We used hydrodynamic gene transfer (HDT) to express X7Ab recombinant antibody *in vivo*. The technique involves the rapid intravenous (i.v.) injection of a large volume of isotonic buffer containing plasmid DNA encoding X7Ab (or

FC-control as a negative control) (Figure 4A). Hepatocytes take up the DNA and transiently overexpress the antibody.²⁴ Plasma from X7Ab HDT-treated mice stained ACKR3/CXCR7-CHO cells, confirming that HDT induced expression and secretion of X7Ab protein *in vivo* (Figure 4B). The plasma C_{max} of X7Ab protein following HDT was four times higher than the plasma C_{max} following injection of recombinant protein (2.4 mg/kg, a clinical dose of Rituximab), and the levels were durable, remaining elevated for >14 days, with a post- C_{max} $t_{1/2}$ of 10 days (Figure 4C).

Assessment of X7Ab Safety *In Vivo*

Given that X7Ab binds to mouse ACKR3 protein, we utilized WT C57BL/6 mice to explore possible *in vivo* toxicity associated with X7Ab treatment. We injected mice with 2.4 mg/kg recombinant

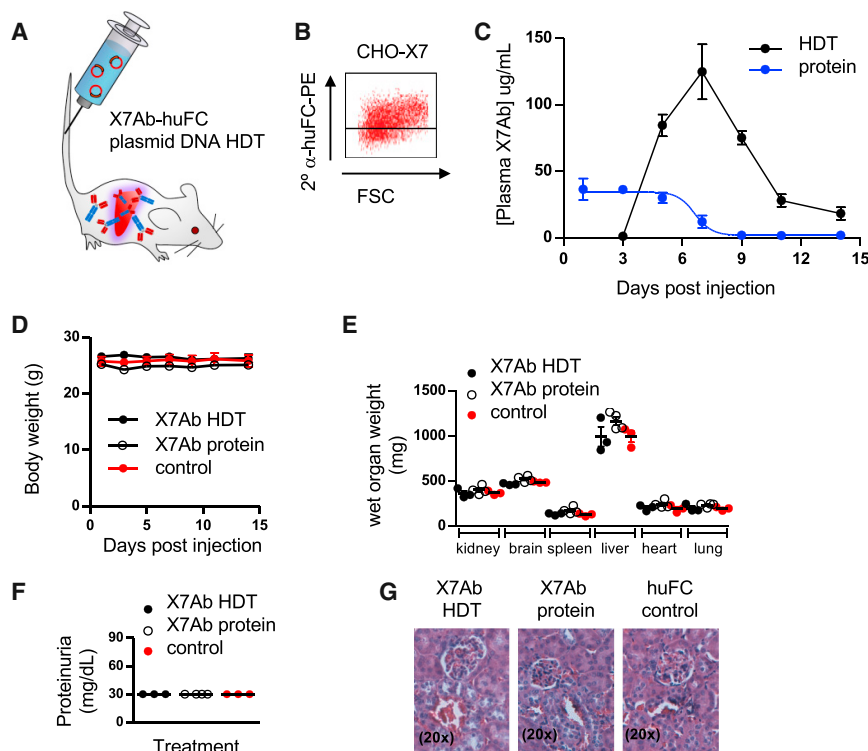


Figure 4. HDT: An Effective Method to Overexpress and Evaluate scFV-FC Antibodies *In Vivo*

(A) HDT is achieved by the rapid (3–5 s) i.v. injection of 10 µg X7Ab plasmid DNA in 2 mL saline. The high venous pressure enables the uptake and overexpression of X7Ab protein by hepatocytes, which is secreted into plasma. (B) Plasma (1:10 dilution) from X7Ab HDT mice stains a ACKR3+ CHO transfectant cell line, determined by flow cytometry following incubation with secondary anti-human FC PE (the bisecting line indicates FC-control staining). (C) Plasma pharmacokinetics of X7Ab. WT mice were injected with either 2.4 mg/kg recombinant X7Ab protein (blue) or 10 µg plasmid DNA by HDT (black) on day 0. Plasma was collected on the indicated days, and the levels of huFC were determined by ELISA, mean ± SEM, n = 3 to 4 mice/group. (D–G) Preclinical safety assessment in rodents: WT C57BL/6 mice were injected with either recombinant X7Ab protein i.v. (2.4 mg/kg) or 10 µg plasmid DNA by HDT on day 0, monitored, and euthanized on day 14. Control mice were injected with Rituximab, which is not known to cause organ toxicity. (D) No differences in body weight; (E) vital organ wet weight (or gross histopathology, not shown); or (F) proteinuria (urine protein ≤ 30 mg/dL by Albutix on day 14). (G) No histological evidence of glomerular inflammation (8-µm sections, H&E, 20× magnification).

X7Ab protein i.v. or 10 µg plasmid DNA by HDT. There was no evidence of acute toxicity immediately following injection; no differences in body weight over a 2-week period between the X7Ab treatment mice and control mice (Figure 4D); and no differences in general appearance or attitude. At the conclusion of the study on day 14, the mice were euthanized and major organs were weighed and examined for gross pathology. There were no differences in vital organ wet weights or appearance (Figure 4E). There was no evidence of overt proteinuria on day 14 (Figure 4F). Given the potential expression of ACKR3 by renal progenitor cells,²⁵ the kidneys were further evaluated for evidence of histopathology, of which none was observed (Figure 4G). Thus, our findings did not identify major toxicity associated with X7Ab in mice.

X7Ab-TMZ Combination Significantly Slows Cancer Progression

To assess the efficacy of X7Ab *in vivo*, we used orthotopic xenograft tumor models of human GBM (U343Luc and U251X7Luc) in SCID mice. ACKR3 expression is retained *in vivo*, as determined by X7Ab staining of resected U251X7 tumor sections (Figure 5A). We confirmed that X7Ab gained access to the brain during GBM tumorigenesis *in vivo* by quantifying antibody levels in brain/GBM homogenates following HDT injection (Figure 5B). In separate cohorts of GBM (U251X7Luc) xenografted mice (SCID and RAG KO), the animals were treated with X7Ab or FC-control HDT 3 and 5 weeks after tumor implantation. X7Ab treatment significantly reduced the tumor burden on week 6, as determined by quantification of total radiance

(flux measured in photons/s) by *in vivo* imaging system (IVIS) imaging following luciferase substrate injection (Figure 5C). Immunodeficient mice with human GBM (U343Luc) tumors were treated with either FC-control or X7Ab DNA by HDT. Mice were imaged on weeks 3, 6, and 9. Two out of five X7Ab HDT mice showed reduced cancer progression on week 9 compared with their signal intensities on week 3 (Figure 5D).

We asked if combination therapy could prolong survival *in vivo*. SCID mice with orthotopic human GBM (U251X7Luc) tumors were treated with either X7Ab via HDT, TMZ, or the combination of X7Ab HDT and TMZ on week 3 after tumor implantation. Compared with control (huFC HDT treated) mice, only the combination therapy significantly extended survival (Figure 5E). The combination group had statistically significant better survival compared to all other groups: TMZ+X7 versus TMZ, *p = 0.0147; TMZ+X7 versus X7, *p = 0.0448; and TMZ+X7 versus FC-control, **p = 0.0041. Although no mice died in the combination group during the study, the tumors in the combination group eventually grew and the mice were euthanized by day 128, the humane endpoint of the experiment. The longest-lived control mouse lived 25 days less or about 20% less time than the longest-lived combination-treated mouse.

X7Ab Significantly Slows Syngeneic Mouse Glioma Progression

To assess the efficacy of X7Ab in an immunocompetent system, we used the GL261 mouse glioma model. We used 15 and 50 mg/kg TMZ as optimal survival and tumor reduction doses based on

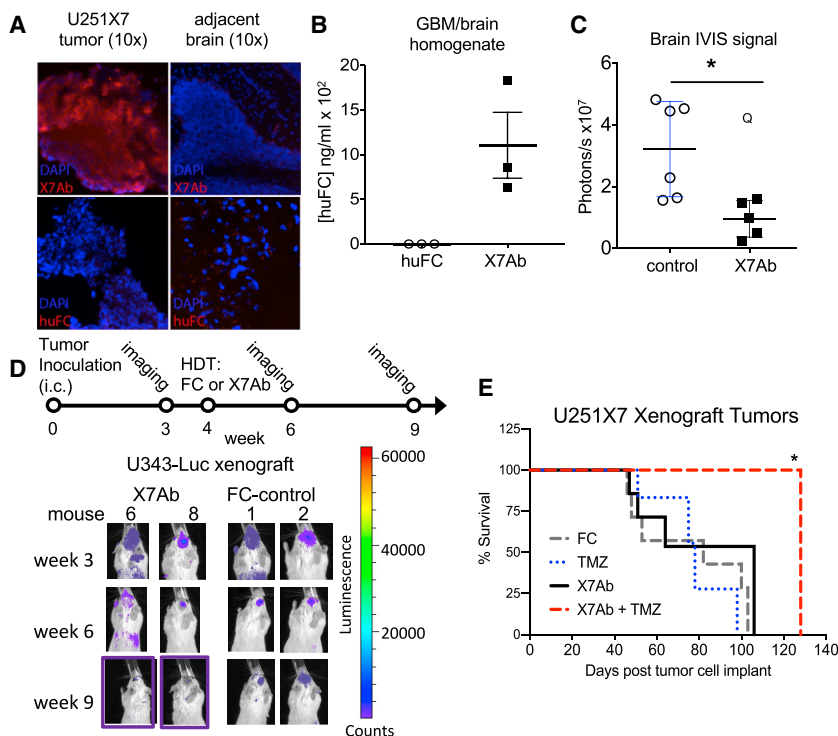


Figure 5. Xenograft Tumor Models: X7Ab HDT Treatment Slows Cancer Progression

Immunodeficient mice were injected orthotopically with 0.3 million human GBM cells (stereotaxic injection into the frontal cortex). (A) GBM xenografts retained ACKR3 expression. Immunofluorescence staining of resected human U251X7Luc glioblastoma tumor cells and adjacent uninjured brain. Brains with tumor lesions were harvested, sectioned, and stained with X7Ab or IgG1-huFC (isotype control) and counterstained with DAPI (blue indicates nuclei). (B) Post-mortem detection of X7Ab antibody in the brains of mice with GBM. (C) X7Ab HDT significantly reduces tumor burden. Xenografted mice were treated with either FC-control or X7Ab HDT on weeks 3 and 5 and tumor radiance (proportional to tumor size) was monitored by IVIS imaging following coelenterazine injection (i.v.) on week 6. $n = 6$ mice per group (3 SCID and 3 RAG each treatment). * $p < 0.05$ by Student's *t* test. The tumor radiance from one mouse was determined to be an outlier by Dixon's Q-test (95% confidence), indicated by the "Q" symbol. (D) Combination therapy of X7Ab HDT and TMZ significantly prolongs survival in a GBM model. Xenografted (U251X7Luc) SCID mice were treated with either FC-control or X7Ab HDT and/or TMZ (5 mg/kg i.p. weekly). $n = 6-8$ mice per group, two biological replicates. * $p < 0.05$ by Gehan-Breslow-Wilcoxon test. (E) SCID mice were injected orthotopically with 0.3 million U343Luc human GBM cells, and tumor progression was monitored by IVIS imaging following coelenterazine injection (i.v.). Xenografted mice were treated with either FC-control or X7Ab HDT on week 3 and imaged again on weeks 6 and 9. A total of 10 mice were xenografted with U343-Luc cells (5 treated with FC-control and 5 treated with X7Ab). The two mice with the smallest tumors in each treatment group are shown.

previous studies,²⁶ and the sub-optimal dose of 5 mg/kg TMZ in combination with X7Ab or FC-control to test the hypothesis that the combination allows us to reduce the dose of TMZ in order to lower the adverse effects associated with TMZ therapy. Using MRI, statistically significant tumor reduction was observed in mice treated with either TMZ at any dose (5, 15, and 50 mg/kg) or X7Ab (10 μ g) or the combination of X7Ab + TMZ 5 mg/kg compared to the huFC only or 10% Captisol vehicle controls (Figures 6A and 6B; Movies S1, S2, S3, S4, S5, S6, S7, S8, and S9), as determined by one-way ANOVA. Decreased tumor burden correlated with increased survival (Figure 6D) in the survival plot of a total of 23 C57BL/6 mice inoculated with GL261 cells. The survival curve includes the control (Ctrl) group: 7 untreated, 1 treated with 10% Captisol vehicle, and 2 treated with huFC (10 μ g); FC + TMZ group: 2 mice treated with huFC (10 μ g) + TMZ 5 mg/kg; TMZ Tx groups: 2 mice treated with TMZ 15 mg/kg and 2 mice treated with TMZ 50 mg/kg; X7Ab group: 3 mice treated with X7Ab (10 μ g); and X7Ab + TMZ group: 4 mice treated with X7Ab (10 μ g) + TMZ 5 mg/kg. The survival curves (Ctrl group versus any of the treatment groups, including the double treatment group) were significantly different by log rank (Mantel-Cox) test: *** $p = 0.0092$; log rank test for trend, ** $p = 0.0044$; and Gehan-Breslow-Wilcoxon test, * $p = 0.0121$.

We analyzed the brain tumor microenvironment at day 28 post tumor cell inoculation by flow cytometry (Figures 6C and 6E). By day 28, all

mice with any of the X7, TMZ, or combination treatments were bright, active, and responsive, whereas the surviving FC-control mice and the 10% Captisol (vehicle control) were moribund, reaching the humane endpoint of the experiment. The samples were analyzed for presence of the relevant tumor-infiltrating leukocytes involved in tumor rejection: NK cells, NKT cells, macrophages, dendritic cells, and T cells (gating strategies, Figures S7 and S8). We found no significant differences among cell population numbers at this time point. However, we found that the combination of X7Ab + TMZ significantly increased the mean fluorescence intensity (MFI) of the M1 polarized macrophage population (Figure 6E). A similar, although not statistically significant, trend of major histocompatibility (MHC)II activation was identified on the dendritic cell population.

DISCUSSION

ACKR3 correlates with poor survival of high-grade glioma patients and, interestingly, is highly expressed in a GBM patient population refractory to treatment (Figure 1B). We also identified significant upregulation of ACKR3-associated molecular partners in GBM. GBM turns resistant to most cytotoxic agents, with hypoxia playing a significant role in both resistance to treatment and poor outcomes.¹ Hypoxia and other inflammatory factors that drive cell survival and stress responses upregulate ACKR3, along with many factors within the tumor and its vasculature.^{27,28} Consistent with the hypoxia link, we also found that ACKR3 falls within a hallmark hypoxia gene-set-related

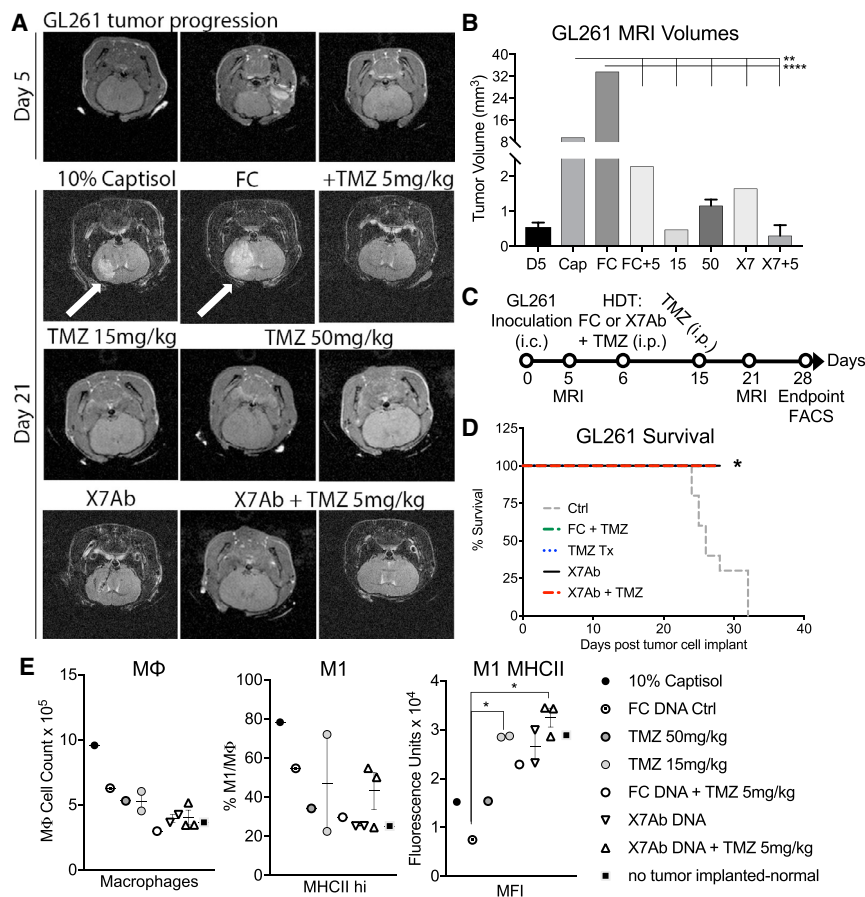


Figure 6. X7Ab HDT Treatment Slows Syngeneic Mouse Glioma Progression

C57BL/6 immunocompetent mice were injected i.c. with 2 μ L of GL261 cell pellet (stereotaxic injection into the frontal cortex). (A) Coronal images acquired at day 5 (D5) or day 21 post tumor implantation between slice 7 and 10 in each mouse. Representative mice from each treatment group are shown. (B) MRI-derived GL261 tumor volume quantification. (C) Treatment timeline for the GL261 model. After initial day 5 verification of tumor take by MRI, mice were treated with antibodies via HDT, TMZ, or the combination of both. (D) Survival plot of a total of 23 C57BL/6 mice inoculated with GL261 cells. Tumor-bearing control (Ctrl) group includes 7 untreated, 1 treated with 10% Captisol vehicle, and 2 treated with huFC (10 μ g). FC + TMZ group is 2 mice treated with huFC (10 μ g) + TMZ 5 mg/kg. TMZ Tx groups are 2 mice treated with TMZ 15 mg/kg and 2 mice treated with TMZ 50 mg/kg. X7Ab group is 3 mice treated with X7Ab (10 μ g). X7Ab + TMZ group is 4 mice treated with X7Ab (10 μ g) + TMZ 5 mg/kg. (E) FACS analysis of digested tumor-inoculated brains at day 21, n = 1–3 from each group. Treatment differences in M1 macrophage activation, quantified by the MHCII MFI from the M1 gate (Figure S7).

module in weighted gene co-expression network analysis (WGCNA) of TCGA GBM samples^{29–31} (Figure S5). These results suggest that ACKR3-targeted immunotherapeutic intervention may be particularly beneficial for patients who respond poorly to standard of care therapy.

To determine whether ACKR3 may be a viable target for precision medicine, we generated a small chimeric antibody capable of mobilizing anti-tumor mechanisms. Previous methods to target ACKR3 consisted of small molecule targeting and single variable domain nanobodies that showed promising therapeutic effects for ACKR3+ cancers.^{4,32,33} Compared with chemotherapy drugs or small molecules, naked mAbs have fewer off-target effects due to their increased target specificity. Antibodies activate innate immune processes, such as ADCC, CDC, and ADCP, and, due to their evolution-optimized properties, are biologically active *in vivo* longer. A recent study successfully targeted ACKR3+ tumors *in vivo* for positron emission tomography (PET) imaging using the radio-labeled antibody clone 11G8, although no therapeutic benefit was reported,³⁴ which is not surprising because 11G8 is a mouse IgG₁ (mIgG₁) isotype and therefore elicits low-level ADCC (Figure S6³⁵).

ADCC is a major mechanism of action for many anti-cancer antibodies, with NK cells being a major contributor of cytotoxicity.²²

ADCC depends upon interactions between the antibody FC domains and FC receptors expressed by specific leukocyte populations. Human NK cells express the A (transmembrane) isoform of CD16 (FcR1IIIA). FC-mediated engagement of CD16 on NK cells leads to an activation cascade that triggers NK-driven cell lysis of antibody-coated target cells.^{22,35} Therefore, antibody efficiency is largely dependent on the interaction between the antibody FC domain and CD16 on the effector cells.²² We demonstrate that X7Ab mediates robust ADCC. Low-grade lymphoma patients with the homozygous higher affinity (V/V) polymorphism exhibit improved clinical response rates compared with those possessing the lower affinity (V/F or F/F) polymorphism after treatment with Rituximab. Using an *in vitro* model of human NK-CD16 polymorphic variants,²² we showed that X7Ab mediated NK-cell-ADCC response, regardless of the high or low affinity variant.

Consistent with other reports indicating that Rituximab kills mainly by ADCC, but also via a weaker CDC response,^{36,37} X7Ab induced a small but statistically significant CDC response against GBM cells. We used rabbit serum (reported to have strong *in vitro* complement activity)³⁸ as well as human serum effector humors. We also asked whether X7Ab has the capacity to engage macrophages because Rituximab and Herceptin also use this mechanism for cytotoxicity.^{39,40} X7Ab significantly enhanced phagocytic activity *in vitro*, which may have substantial and beneficial downstream effects *in vivo*. In enhancing phagocytosis, X7Ab may facilitate tumor antigen presentation to the adaptive immune system, thereby helping immune

recognition of tumor cells for enhanced patient response and long-term anti-tumor immunity.

Although X7Ab specifically blocked CXCL12 signaling, it did not directly induce apoptosis, implying perhaps that GBM tumor cells do not require ACKR3-dependent survival signals. On the other hand, inhibition of ligand signaling may potentially sensitize ACKR3+ cells to chemotherapeutics. In line with the observation of ACKR3 being highly expressed in a TMZ-refractory GBM patient population, we tested the hypothesis that the combination of X7Ab with TMZ, a first-line GBM treatment, would result in improved efficacy, given that the agents act via non-overlapping mechanisms. X7Ab combined with TMZ induced significantly more target GBM cell death than either agent alone via both ADCC and CDC mechanisms *in vitro*. Our *in vitro* data establish the cellular killing mechanisms employed by X7Ab (ADCC, CDC, and ADCP) to effectively mobilize anti-tumor immune effectors and kill tumor cells either alone, or, more effectively, in combination with TMZ.

An additional innovative feature of this study was the establishment of a novel platform based on HDT to enable the expression of recombinant antibodies *in vivo*. The method recapitulates certain aspects of virally delivered gene therapy. An advantage of HDT is that it does not require production of large amounts of recombinant protein for testing *in vivo*. The *in vivo* overexpression of antibodies by HDT (enabled by the single chain FV-FC format) may prove to be a powerful *in vivo* screening tool for targeted antibody development. HDT embodies aspects of passive immunity, in that the body is transiently receiving antibodies unable to undergo affinity maturation.

Although SCID mice have no T or B cells, they have active innate immunity components, including NK cells, macrophages, and a complement system. Of note, we used a suboptimal dose of TMZ in order to reduce the TMZ-associated side effects and better model patients refractory to TMZ, and this group did not have significantly improved survival. The combination group had statistically significant improved survival compared to all the other groups. The inherent leakiness of the tumor vascular endothelium likely permits our small single chain antibody to penetrate the tumor tissue. The non-overlapping mechanisms of action of X7Ab (FC receptor mediated) and TMZ (DNA damage response mechanism) work together in contributing improved survival.

The GL261 mouse glioma is a robust standardized mouse syngeneic model, with survival time for mice after GL261 cell implantation ranging from 17 to 37 days.^{41,42} Compared to the negative control groups, treatment with X7Ab alone, TMZ alone, or the combination of X7Ab with TMZ significantly inhibited tumor growth by day 21, as quantified by MRI segmentation to give tumor volumes. Although the combination of X7Ab with TMZ at the low dose of 5 mg/kg was not statistically better than TMZ alone, or X7 alone, there was a downward trend, with the combination being best at reducing tumor burden. This suggests that using X7Ab would allow us to decrease the dosage of TMZ 3–10x, thus minimizing toxic side effects.

Fluorescence-activated cell sorting (FACS) analysis at day 28 allowed *in vivo* post treatment analysis of the tumor microenvironment; however, it is likely that at this time point, many of the tumor-fighting cells involved in the initial therapy-mediated anti-tumor response were missed. From all the tumor-infiltrating leukocytes involved in tumor rejection (NK cells, NKT cells, macrophages, dendritic cells, and T cells) that were analyzed, only the M1 macrophages demonstrated significant differences at this time point. M1 macrophages, when polarized by expressing higher levels of MHCII, can support anti-tumor immune responses.⁴³ TMZ significantly increased MHCII activation, and although X7Ab increased the MHCII MFI of M1 macrophages, combining X7Ab with a low dose of TMZ at 5 mg/kg activated M1 macrophages the most. These *in vivo* findings suggest X7Ab can induce upregulation of MHCII expression on M1 macrophages and likely dendritic cells to potentiate the polarization/activation of innate immune cell responders to engage anti-tumor immune defenses *in vivo*. X7Ab may induce this effect alone, but the effect is enhanced when combined with TMZ.

In conclusion, we validated X7Ab as a tool for precision targeted immunotherapy for GBM. We show for the first time a large molecule approach to targeting ACKR3, and that as a therapeutic, it is safe and specific in mice. X7Ab utilizes a wide range of effector functions to engage the immune system to kill tumors, and combines effectively with chemotherapy to improve overall survival in GBM models. Based on this evidence, X7Ab may provide the basis for novel therapeutic interventions for improved survival in GBM patients.

MATERIALS AND METHODS

ACKR3/CXCR7 Survival Correlation and RNA Expression Determination

The survival KM plots, significance, and hazard ratios were generated using PROGene⁴⁴ using the median mRNA expression of CXCR7 to divide patients into either high or low expression. We used mRNA microarray data from the cancer genome atlas TCGA database (<https://tcga-data.nci.nih.gov/docs/publications/tcga/>; accession date 05/30/2016). TCGA GBM level 3 data representing normalized gene-level expression signals were downloaded and analyzed using GraphPad Prism Software. The gene expression measurements were provided as the Log₂ normalized ratio of expression in the tumor compared to normal brain tissue (TCGA normal organ: brain).

Cells and Reagents

U251, U343, GL261, RAW264.7, and U937 cells were obtained from the American Type Culture Collection. U251LucX7 (ACKR3 transfectants) were generated using ACKR3 plasmid DNA using lipid transfection (Lipofectamine 2000) following the manufacturer's protocol and selected by antibiotic resistance. HUVECs were obtained from Lonza, cultured per the manufacturer's specifications, and used at passage 3. The Chinese hamster ovary (CHO) cells expressing modified ACKR3 β-arrestin2 were obtained from DiscoveRx and cultured in Ham's F-12 medium (Mediatech) containing 10% fetal

bovine serum (FBS) (Gemini Bio-Products), penicillin/streptomycin (Mediatech), 0.3 mg/mL hygromycin (Invitrogen), and 0.8 mg/mL G-418 (Mediatech). The CD16-transduced NK-92 cell lines, 176F NK-92.05 and 176V NK-92.05, were a generous gift from Kerry S. Campbell, Fox Chase Cancer Center. CXCL12 was purchased from R&D Systems. 11G8 and isotype control mouse IgG1 was provided by ChemoCentryx (Mountain View, CA), whereas X7Ab and huFC control were generated and provided by LakePharma (Belmont, CA). TMZ, Sigma-Aldrich, was injected at 5 mg/kg intraperitoneally (i.p.) once per week for 5 weeks, starting treatment at week 3 after tumor cell implantation.

Binding Affinity (K_D) Determination for X7Ab

An Octet Qke system using anti-human FC biosensors was used to measure the kinetics of association and dissociation of X7Ab and its ACKR3 antigen (by surface-based biolayer interferometry). X7Ab (20 μ g/mL) was loaded on the biosensor, and its association with various concentrations of ACKR3 antigen (300, 100, 33.3, and 11.1 nM) was measured over 180 s. Dissociation was monitored for 300 s. Reference subtraction, Savitsky Golay filtering, and global fitting of kinetic rates for the association and dissociation were performed using FortéBio analysis software.

Flow Cytometry

2.5×10^5 cells were used for each staining. For unconjugated antibodies (Abs), cells were incubated with the indicated primary Abs at 4°C for 30 min in 100 μ L PBS/2% FBS/2% goat serum. Cells were washed with PBS and centrifuged for 3 min at 1,200 rpm. Following the washing step, cells were incubated with secondary goat anti-mouse PE (R&D Systems) in 50 μ L PBS/2% FBS/2% goat serum. For directly conjugated Abs, cells are incubated with labeled Ab at 4°C for 30 min in 100 μ L PBS/2% FBS/2% goat serum. Cells were washed and centrifuged for 3 min at 1,200 rpm, resuspended, and fixed in 200 μ L PBS/1% paraformaldehyde and were analyzed using a FACSCalibur (BD Biosciences, Franklin Lake, NJ).

Immunofluorescence

U251X7 tumor-positive brains isolated from SCID (severe combined immunodeficiency) mice were placed in Tissue-Tek compound (Sakura) and frozen at -80°C . Cryosections of tissues fixed in 4% paraformaldehyde were stained with X7Ab or FC-control (at 10–25 μ g/mL). Staining was imaged on a fluorescent microscope (Carl Zeiss) at 10x.

β -Arrestin Assays

2×10^4 CHO-ACKR3- β gal1: β -arrestin2- β gal2 (CHO-X7) cells (DiscoveRx) were seeded into 96-well plates and cultured overnight. The next day, the medium was removed by aspiration, 100 μ L of PBS containing varying concentrations of ligands was added to the wells, and the plates were incubated in 5% CO_2 at 37°C. After 90 min, 50 μ L of β -galactosidase (β -gal) substrate (DiscoveRx) was added to the wells and the plates were incubated at room temperature. After 1 hr, light emission (absorbance) was analyzed in a bench top plate

reader, Molecular Devices SpectraMax M5. For Ab-blocking studies, the cells were preincubated with Abs for 30 min in 5% CO_2 at 37°C, and then 5 μ L of chemokine agonist was added, and the plates were processed as described.

ADCC Assay

Tumor cell line targets were labeled with CFSE (carboxyfluorescein succinimidyl ester), incubated with the indicated antibodies for 30 min, and then mixed with human PBMC, mouse splenocytes, or NK cell effectors at the indicated effector:target (E:T) ratios. The NK effector cells had been previously cultured overnight with interleukin-2 (IL-2). Propidium iodide (PI) was added to the cell mixture after 18 hr, and the cells were assessed by flow cytometry by evaluating the % of PI+ CFSE+ cells of total CFSE+ cells. For combined TMZ experiments, U251X7 cells were incubated \pm TMZ (6 μ M) for 5 days, labeled with CFSE, incubated \pm X7Ab (100 μ g/mL) for 30 min, and then mixed with human PBMC effectors at an E:T ratio of 30:1. PI was added to the cell mixture after 4 hr, and the % viable cells (PI negative) was assessed by flow cytometry by evaluating the % of PI– CFSE+ cells of total CFSE+ cells. The data were normalized to the average of the total number of viable targets in the untreated wells (set to 100% viable cell targets). For ADCC using SCID splenocyte effectors, U251X7 cells were incubated \pm TMZ (3 μ M) for 3 days, labeled with CFSE, incubated \pm X7Ab (100 μ g/mL) for 30 min, and then mixed with SCID mouse splenocyte effectors at an E:T ratio of 100:1. PI was added to the cell mixture after 18 hr, and the % viable cells (PI negative) was assessed by flow cytometry by evaluating the % of PI– CFSE+ cells of total CFSE+ cells. The data were normalized to the average of the total number of viable targets in the untreated wells (set to 100% viable cell targets).

CDC Assay

Tumor targets were incubated with the indicated antibodies for 20 min at room temperature and then mixed with rabbit or human serum (1:4 final dilution in Hank's balanced salt solution [HBSS]) for 18 hr at 37°C. CDC was assessed by flow cytometry by evaluating the percentage of PI-positive cells.

ADCP Assay

Tumor cell line targets were labeled with CFSE, incubated with the indicated antibodies for 30 min, and then mixed with effector cells, human monocyte line U937, or mouse line RAW264.7 at an E:T ratio of 5:1 for 4 hr. RAW cells were stimulated with LPS (100 ng/mL) 18 hr before use, and U937 cells were differentiated into macrophages using PMA (100 ng/mL) for 48 hr, followed by a resting period of 24 hr before use. The effector cells were labeled with an FL-4 dye. Cells were assessed by flow cytometry by evaluating the % of FL4+ CFSE+ cells as the % phagocytosed in the total population.

Apoptosis Assays

2×10^4 cells were plated and incubated for 18 hr with dilutions of the antibody. Cell viability was assessed by double staining of annexin-V fluorescein isothiocyanate (FITC)/PI. Cells were then analyzed using

a FACScan with Cell Quest software (Beckton Dickinson) for acquisition and analysis.

Mice and Animal Care

6- to 8-week-old female WT C57BL/6, Rag-deficient, and BALB/c SCID mice were purchased from Jackson Laboratories (Bar Harbor, ME, USA) and used for the experiments as described in the figure legends. Experiments and procedures were approved by the VAPAHCS Institutional Animal Use and Care Committee. For SCID survival studies, the mice were sacrificed when the mice reached the humane endpoint of tumor burden. MRI studies were approved by the Stanford Administrative Panel on Laboratory Animal Care and conducted at the Preclinical Imaging Core Facility at the Canary Center at Stanford for Cancer Early Detection.

Treatment *In Vivo*

Mice were anesthetized and tumor cells were stereotaxically injected into the striatum using a Hamilton syringe. Coordinates relative to bregma were the following: posterior = 1.95 mm, lateral = 1.75 mm, and ventral = 0.85 mm. SCID balb/c mice were injected orthotopically with $\sim 3 \times 10^5$ U343 human GBM cells, and tumor progression monitored by IVIS imaging following coelenterazine injection (i.v.). Xenografted mice were treated with either FC-control or X7Ab HDT on week 3 and imaged again on weeks 6 and 9. A total of 10 mice were xenografted with U343-Luc cells (5 treated with FC-control and 5 treated with X7Ab). The same procedure was used for implanting U251LucX7 cells. Treatment was started at 3–6 weeks after the injection of tumor cells once mice developed luciferase signals as baseline levels of tumor lesion. Tumor-bearing mice were randomized into control and treatment groups, and five to six mice were used for each experimental cohort. Mice were followed to their endpoints (30–128 days). TMZ, Sigma-Aldrich, was injected at 5 mg/kg i.p. once per week for 5 weeks, starting treatment at week 3 after tumor cell implantation. For syngeneic studies, C57BL6 immunocompetent mice were injected intracranially (i.c.) with 2 μ L of GL261 cell pellet (stereotaxic injection into the frontal cortex), as described above. Control group: 7 mice with tumors but untreated, 10% Captisol was used as the TMZ vehicle control, and 2 mice were treated with huFC (10 μ g) alone; FC + TMZ group: 2 mice were treated with huFC (10 μ g) + TMZ 5 mg/kg; TMZ Tx groups: 2 mice were treated with TMZ 15 mg/kg and 2 mice were treated with TMZ 50 mg/kg; X7Ab group: 3 mice were treated with X7Ab (10 μ g); X7Ab + TMZ group: 4 mice were treated with X7Ab (10 μ g) + TMZ 5 mg/kg.

HDT

Mice were injected with either recombinant X7Ab protein i.v. (2.4 mg/kg) or 10 μ g plasmid DNA by HDT on day 0. HDT was performed as previously described.⁴⁵ In brief, plasmid DNA was diluted in 2 mL physiological saline solution and injected i.v. (tail vein) in 3–5 s.

In Vivo Bioluminescence Imaging

U343-Luc and U251X7-Luc glioma-bearing mice were injected i.v. with coelenterazine (15 μ g/mouse). 5 min later, mice were anaesthe-

tized and processed for image analysis using a Xenogen IVIS Lumina imaging system (Caliper, PerkinElmer) for 1–5 min. Tumor growth was imaged once a week starting on day 5 post implantation until mice reached a humane endpoint. Imaging data were analyzed and quantified with the Living Image Software for IVIS Lumina II (PerkinElmer).

Detection of X7Ab Antibody in the Brains of Mice with GBM

RAG and SCID mice were injected orthotopically with $\sim 3 \times 10^5$ U251X7Luc human GBM cells. Xenografted mice were left untreated or treated with X7Ab HDT on week 3 and week 5. On week 6, the mice were euthanized, exsanguinated, and perfused with 30 mL PBS. The brain and implanted tumor were removed and homogenized in 4-mL protease inhibitor buffer. Following high-speed centrifugation, the clarified extract was subjected to ELISA to detect human FC (limit of detection = 10 ng/mL).

Immunohistochemistry

Glioma and control specimens were fixed in 10% formaldehyde and embedded in paraffin. Brain sections (12 μ m) were deparaffinized, and antigen retrieval was performed. After 3 washes with 1x Tris-buffered saline and Tween 20 (TBST) solution, slides were incubated at room temperature with corresponding species-specific horseradish peroxidase (HRP) conjugated secondary antibody (Dako) for 2 hr or from Vector Laboratories (1:200) for 30 min. Signal was visualized by the HRP-DAB reaction and counterstained with hematoxylin.

MRI

The mice were anesthetized in a knockdown box with 3% isoflurane, and then placed on a MRI-compatible cradle connected to a ventilator with 1.3%–1.5% isoflurane. A fiber-optic temperature probe and respiratory sensor were placed adjacent to the abdomen of the mouse. The mouse was inserted into a mouse head RF coil. The coil with the mouse was inserted to the iso-center of the magnet of a 3.0-T MR Scanner (Signa Excite HD 3T; GE Healthcare, Milwaukee, WI). Heated air was pumped into the bore to maintain the mouse body temperature at physiological levels (34°C–38°C). Morphological T1- and T2-weighted magnetic resonance whole brain images were collected using MR Solutions software (Guildford, UK), and tumor volume was quantified using region of interest (ROI) segmentation using OsiriX MD (Pixmeo, Geneva, Switzerland), where the volume from each axial slice where the tumor appeared within the brain was integrated/quantified by the ROI volume-compute volume function.

Flow Cytometry of GL261 Inoculated Mouse Brains

On day 28 post tumor cell inoculation, mice were terminated and the brains of the treatment groups and one tumor-free (normal) littermate were dissected and immediately transferred in ice-cold HBSS. Brains were digested in a buffer solution containing HBSS, Collagenase P (0.2 mg/mL), Dispase II (0.8 mg/mL), DNase I (0.01 mg/mL), and Collagenase A (0.3 mg/mL) for 60 min at 37°C under gentle rocking as described before.⁴¹ Briefly, the digested cells were pre-incubated with rat anti-mouse Fc γ III/II receptor (CD16/CD32) blocking antibody for 5 min at 4°C, and then stained with the fluorochrome-conjugated

antibodies (1:100). PI (1:3,000; Thermo Fisher Scientific) was added for live gating. Flow cytometry was performed using FACSDiva software on a LSRII (BD Biosciences; San Jose, CA, USA) and analyzed using FlowJo software (Tree Star; Ashland, OR, USA).

The cells were stained with anti-mouse antibody cocktail: CD45 AF700 (clone 30-F11, eBioscience), Gr-1 PerCP Cy5.5 (clone RB6-8C5, BioLegend), CD11b V500 (clone M1/70, BD), CD11c PE Cy7 (clone N418, BioLegend), F4/80 APC Cy7 (clone BM8, BioLegend), CD206 BV421 (clone C068C2, BioLegend), MHC class II PE-Cy5 (clone M5/114.15.2, eBioscience), T cell receptor (TCR)- β FITC (clone H57-597, BioLegend), and NK1.1 APC (clone PK136, BioLegend).

Weighted Gene Co-expression Network Analysis

TCGA GBM mRNASeq Archives from 171 patient tumor samples were downloaded from Firehose (<http://gdac.broadinstitute.org>). We used the WGCNA package and tutorial^{29,46} to build a weighted gene co-expression network that contains 20,502 nodes (genes). The soft-thresholding power of 9 for weighted network construction was selected to maintain both the scale-free topology and sufficient node connectivity, as recommended in the WGCNA manual. We identified the modules using the advanced dynamic tree cut technique, built with the default value of SplitDepth for robust module detection in WGCNA and block-wise network construction and module detection. Genes were clustered into two blocks with a size of 10,251 genes. We then performed a full network analysis in each block separately to determine modules, represented by colors. Modules contain the gene networks. The blue module where ACKR3 was found was then submitted to Gene Set Enrichment Analysis (GSEA) (<http://software.broadinstitute.org/gsea/login.jsp?sessionId=2759025EB5AA18A7B83495B7C8C3C49F>) to determine ACKR3 gene/module biological relevance (Tables S1 and S2).

Statistical Analysis

All statistical significance was determined using GraphPad Prism 6 (GraphPad Software). Statistical significance was determined using unpaired two-tailed Student's t test or ANOVA in GraphPad Prism 6 (GraphPad Software), unless otherwise noted. Data are significant when $p \leq 0.05$; * $p \leq 0.05$, ** $p \leq 0.01$, *** $p \leq 0.001$, and **** $p \leq 0.0001$. Sample sizes and animal numbers were chosen based on power calculations of 0.8 and pilot studies performed in the laboratory. For TCGA and ADCP multi-group analysis, significance levels were determined with GraphPad Prism 6 using grouped analysis, two-way ANOVA, and Dunnett's multiple comparisons test.

SUPPLEMENTAL INFORMATION

Supplemental Information includes eight figures, two tables, and nine movies and can be found with this article online at <https://doi.org/10.1016/j.ymthe.2018.02.030>.

AUTHOR CONTRIBUTIONS

Conceived and Designed the Experiments, B.A.Z., N.S., A.S., H.T.; Performed the Experiments, N.S., J.C.C., K.H., Y.Z., C.O., J.G.,

A.D.J., T.M.B., S.L., S.H., L.N., J.K.; Analyzed the Data, N.S., K.H., M.M., E.C.B., H.T., B.A.Z.; Contributed Reagents/Materials/Analysis Tools, K.H., E.C.B., H.T.; Wrote the Paper, N.S., E.C.B., B.A.Z.

CONFLICTS OF INTEREST

K.H. and H.T. are employees of LakePharma, Inc. The other authors have declared that no competing interests exist.

ACKNOWLEDGMENTS

The authors thank Dr. Kerry Campbell at Fox Chase Cancer Center and NantKwest, Inc., for generously providing human NK cell lines and Dr. Dmitry Velmeshev for careful reading and suggestions to improve the manuscript. This work was supported by the NIH (3R01AI079320 to B.A.Z.; R01CA169354 and R01GM037734 to E.C.B.; and the Emerson Collective Cancer Research Fund to B.A.Z. and E.C.B.). N.S. was supported by a diversity supplement from the NIH (3R01CA169354-03S1). T.M.B. was supported by a diversity supplement from the NIH (3R01AI079320-03S1). M.M. thanks the Luxembourg National Research Fund (FNR PEARL P16/BM/11192868) for support.

REFERENCES

- Cavazos, D.A., and Brenner, A.J. (2016). Hypoxia in astrocytic tumors and implications for therapy. *Neurobiol. Dis.* 85, 227–233.
- Liu, Y., Carson-Walter, E.B., Cooper, A., Winans, B.N., Johnson, M.D., and Walter, K.A. (2010). Vascular gene expression patterns are conserved in primary and metastatic brain tumors. *J. Neurooncol.* 99, 13–24.
- Hattermann, K., Held-Feindt, J., Lucius, R., Mürköster, S.S., Penfold, M.E., Schall, T.J., and Mentlein, R. (2010). The chemokine receptor CXCR7 is highly expressed in human glioma cells and mediates antiapoptotic effects. *Cancer Res.* 70, 3299–3308.
- Walters, M.J., Ebsworth, K., Berahovich, R.D., Penfold, M.E., Liu, S.C., Al Omran, R., Kioi, M., Chernikova, S.B., Tseng, D., Mulkearns-Hubert, E.E., et al. (2014). Inhibition of CXCR7 extends survival following irradiation of brain tumours in mice and rats. *Br. J. Cancer* 110, 1179–1188.
- Birner, P., Tchorbanov, A., Natchev, S., Tuettenberg, J., and Guentchev, M. (2015). The chemokine receptor CXCR7 influences prognosis in human glioma in an IDH1-dependent manner. *J. Clin. Pathol.* 68, 830–834.
- Deng, L., Zheng, W., Dong, X., Liu, J., Zhu, C., Lu, D., Zhang, J., Song, L., Wang, Y., and Deng, D. (2017). Chemokine receptor CXCR7 is an independent prognostic biomarker in glioblastoma. *Cancer Biomark.* 20, 1–6.
- Berahovich, R.D., Zabel, B.A., Penfold, M.E.T., Lewén, S., Wang, Y., Miao, Z., Gan, L., Pereda, J., Dias, J., Slukvin, I.I., et al. (2010). CXCR7 protein is not expressed on human or mouse leukocytes. *J. Immunol.* 185, 5130–5139.
- Burns, J.M., Summers, B.C., Wang, Y., Melikian, A., Berahovich, R., Miao, Z., Penfold, M.E., Sunshine, M.J., Littman, D.R., Kuo, C.J., et al. (2006). A novel chemokine receptor for SDF-1 and I-TAC involved in cell survival, cell adhesion, and tumor development. *J. Exp. Med.* 203, 2201–2213.
- Berahovich, R.D., Zabel, B.A., Lewén, S., Walters, M.J., Ebsworth, K., Wang, Y., Jaen, J.C., and Schall, T.J. (2014). Endothelial expression of CXCR7 and the regulation of systemic CXCL12 levels. *Immunology* 141, 111–122.
- Dambly-Chaudière, C., Cubedo, N., and Ghysen, A. (2007). Control of cell migration in the development of the posterior lateral line: antagonistic interactions between the chemokine receptors CXCR4 and CXCR7/RDC1. *BMC Dev. Biol.* 7, 23.
- Boldajipour, B., Mahabaleswar, H., Kardash, E., Reichman-Fried, M., Blaser, H., Minina, S., Wilson, D., Xu, Q., and Raz, E. (2008). Control of chemokine-guided cell migration by ligand sequestration. *Cell* 132, 463–473.
- Sierro, F., Biben, C., Martínez-Muñoz, L., Mellado, M., Ransohoff, R.M., Li, M., Woehl, B., Leung, H., Groom, J., Batten, M., et al. (2007). Disrupted cardiac

- development but normal hematopoiesis in mice deficient in the second CXCL12/SDF-1 receptor, CXCR7. *Proc. Natl. Acad. Sci. USA* 104, 14759–14764.
13. Gerrits, H., van Ingen Schenau, D.S., Bakker, N.E., van Disseldorp, A.J., Strik, A., Hermens, L.S., Koenen, T.B., Krajnc-Franken, M.A., and Gossen, J.A. (2008). Early postnatal lethality and cardiovascular defects in CXCR7-deficient mice. *Genesis* 46, 235–245.
 14. Phillips, H.S., Kharbanda, S., Chen, R., Forrester, W.F., Soriano, R.H., Wu, T.D., Misra, A., Nigro, J.M., Colman, H., Soroceanu, L., et al. (2006). Molecular subclasses of high-grade glioma predict prognosis, delineate a pattern of disease progression, and resemble stages in neurogenesis. *Cancer Cell* 9, 157–173.
 15. Luker, K.E., Gupta, M., and Luker, G.D. (2009). Imaging chemokine receptor dimerization with firefly luciferase complementation. *FASEB J.* 23, 823–834.
 16. Salazar, N., Muñoz, D., Kallifatidis, G., Singh, R.K., Jordà, M., and Lokeshwar, B.L. (2014). The chemokine receptor CXCR7 interacts with EGFR to promote breast cancer cell proliferation. *Mol. Cancer* 13, 198.
 17. Kallifatidis, G., Munoz, D., Singh, R.K., Salazar, N., Hoy, J.J., and Lokeshwar, B.L. (2016). β -arrestin-2 counters CXCR7-mediated EGFR transactivation and proliferation. *Mol. Cancer Res.* 14, 493–503.
 18. Hiratsuka, S., Watanabe, A., Aburatani, H., and Maru, Y. (2006). Tumour-mediated upregulation of chemoattractants and recruitment of myeloid cells predetermines lung metastasis. *Nat. Cell Biol.* 8, 1369–1375.
 19. Murat, A., Migliavacca, E., Gorlia, T., Lambiv, W.L., Shay, T., Hamou, M.F., de Tribolet, N., Regli, L., Wick, W., Kouwenhoven, M.C., et al. (2008). Stem cell-related “self-renewal” signature and high epidermal growth factor receptor expression associated with resistance to concomitant chemoradiotherapy in glioblastoma. *J. Clin. Oncol.* 26, 3015–3024.
 20. Zabel, B.A., Wang, Y., Lewén, S., Berahovich, R.D., Penfold, M.E., Zhang, P., Powers, J., Summers, B.C., Miao, Z., Zhao, B., et al. (2009). Elucidation of CXCR7-mediated signaling events and inhibition of CXCR4-mediated tumor cell transendothelial migration by CXCR7 ligands. *J. Immunol.* 183, 3204–3211.
 21. Shimizu, S., Brown, M., Sengupta, R., Penfold, M.E., and Meucci, O. (2011). CXCR7 protein expression in human adult brain and differentiated neurons. *PLoS One* 6, e20680.
 22. Binyamin, L., Alpaugh, R.K., Hughes, T.L., Lutz, C.T., Campbell, K.S., and Weiner, L.M. (2008). Blocking NK cell inhibitory self-recognition promotes antibody-dependent cellular cytotoxicity in a model of anti-lymphoma therapy. *J. Immunol.* 180, 6392–6401.
 23. Campbell, K.S. (2012). Genetically modified human natural killer cell lines. US patent 8,313,943 B2, filed, July 8, 2005, and granted November 17, 2009.
 24. Suda, T., and Liu, D. (2007). Hydrodynamic gene delivery: its principles and applications. *Mol. Ther.* 15, 2063–2069.
 25. Mazzinghi, B., Ronconi, E., Lazzeri, E., Sagrinati, C., Ballerini, L., Angelotti, M.L., Parente, E., Mancina, R., Netti, G.S., Becherucci, F., et al. (2008). Essential but differential role for CXCR4 and CXCR7 in the therapeutic homing of human renal progenitor cells. *J. Exp. Med.* 205, 479–490.
 26. Hirst, T.C., Vesterinen, H.M., Sena, E.S., Egan, K.J., Macleod, M.R., and Whittle, I.R. (2013). Systematic review and meta-analysis of temozolomide in animal models of glioma: was clinical efficacy predicted? *Br. J. Cancer* 108, 64–71.
 27. Miao, Z., Luker, K.E., Summers, B.C., Berahovich, R., Bhojani, M.S., Rehemtulla, A., Kleer, C.G., Essner, J.J., Nasevicius, A., Luker, G.D., et al. (2007). CXCR7 (RDC1) promotes breast and lung tumor growth in vivo and is expressed on tumor-associated vasculature. *Proc. Natl. Acad. Sci. USA* 104, 15735–15740.
 28. Van Rechem, C., Rood, B.R., Touka, M., Pinte, S., Jenal, M., Guérardel, C., Ramsey, K., Monté, D., Bégue, A., Tschan, M.P., et al. (2009). Scavenger chemokine (CXC motif) receptor 7 (CXCR7) is a direct target gene of HIC1 (hypermethylated in cancer 1). *J. Biol. Chem.* 284, 20927–20935.
 29. Langfelder, P., and Horvath, S. (2008). WGCNA: an R package for weighted correlation network analysis. *BMC Bioinformatics* 9, 559.
 30. Zhang, B., and Horvath, S. (2005). A general framework for weighted gene co-expression network analysis. *Stat. Appl. Genet. Mol. Biol.* 4, e17.
 31. Horvath, S., Zhang, B., Carlson, M., Lu, K.V., Zhu, S., Felciano, R.M., Laurance, M.F., Zhao, W., Qi, S., Chen, Z., et al. (2006). Analysis of oncogenic signaling networks in glioblastoma identifies ASPM as a molecular target. *Proc. Natl. Acad. Sci. USA* 103, 17402–17407.
 32. Oishi, S., Kuroyanagi, T., Kubo, T., Montpas, N., Yoshikawa, Y., Misu, R., Kobayashi, Y., Ohno, H., Heveker, N., Furuya, T., et al. (2015). Development of novel CXC chemokine receptor 7 (CXCR7) ligands: selectivity switch from CXCR4 antagonists with a cyclic pentapeptide scaffold. *J. Med. Chem.* 58, 5218–5225.
 33. Maussang, D., Mujčić-Delić, A., Descamps, F.J., Stortelers, C., Vanlandschoot, P., Stigter-van Walsum, M., Vischer, H.F., van Roy, M., Vosjan, M., Gonzalez-Pajuelo, M., et al. (2013). Llama-derived single variable domains (nanobodies) directed against chemokine receptor CXCR7 reduce head and neck cancer cell growth in vivo. *J. Biol. Chem.* 288, 29562–29572.
 34. Behnam Azad, B., Lisok, A., Chatterjee, S., Poirier, J.T., Pullambhatla, M., Luker, G.D., Pomper, M.G., and Nimmagadda, S. (2016). Targeted imaging of the atypical chemokine receptor 3 (ACKR3/CXCR7) in human cancer xenografts. *J. Nucl. Med.* 57, 981–988.
 35. Nimmerjahn, F., and Ravetch, J.V. (2008). Fc γ receptors as regulators of immune responses. *Nat. Rev. Immunol.* 8, 34–47.
 36. Beum, P.V., Lindorfer, M.A., Beurskens, F., Stukenberg, P.T., Lokhorst, H.M., Pawluczko, A.W., Parren, P.W., van de Winkel, J.G., and Taylor, R.P. (2008). Complement activation on B lymphocytes opsonized with rituximab or ofatumumab produces substantial changes in membrane structure preceding cell lysis. *J. Immunol.* 181, 822–832.
 37. Boross, P., and Leusen, J.H.W. (2012). Mechanisms of action of CD20 antibodies. *Am. J. Cancer Res.* 2, 676–690.
 38. Walford, R.L., Gallagher, R., and Sjaarda, J.R. (1964). Serologic typing of human lymphocytes with immune serum obtained after homografting. *Science* 144, 868–870.
 39. Gül, N., and van Egmond, M. (2015). Antibody-dependent phagocytosis of tumor cells by macrophages: a potent effector mechanism of monoclonal antibody therapy of cancer. *Cancer Res.* 75, 5008–5013.
 40. Petricevic, B., Laengle, J., Singer, J., Sachet, M., Fazekas, J., Steger, G., Bartsch, R., Jensen-Jarolim, E., and Bergmann, M. (2013). Trastuzumab mediates antibody-dependent cell-mediated cytotoxicity and phagocytosis to the same extent in both adjuvant and metastatic HER2/neu breast cancer patients. *J. Transl. Med.* 11, 307.
 41. Scholz, A., Harter, P.N., Cremer, S., Yalcin, B.H., Gurnik, S., Yamaji, M., Di Tacchio, M., Sommer, K., Baumgarten, P., Bähr, O., et al. (2016). Endothelial cell-derived angiopoietin-2 is a therapeutic target in treatment-naïve and bevacizumab-resistant glioblastoma. *EMBO Mol. Med.* 8, 39–57.
 42. Zhang, L., Kundu, S., Feenstra, T., Li, X., Jin, C., Laaniste, L., El Hassan, T.E., Ohlin, K.E., Yu, D., Olofsson, T., et al. (2015). Pleiotrophin promotes vascular abnormalization in gliomas and correlates with poor survival in patients with astrocytomas. *Sci. Signal.* 8, ra125.
 43. Ostrand-Rosenberg, S. (2008). Immune surveillance: a balance between protumor and antitumor immunity. *Curr. Opin. Genet. Dev.* 18, 11–18.
 44. Goswami, C.P., and Nakshatri, H. (2014). PROGeneV2: enhancements on the existing database. *BMC Cancer* 14, 970.
 45. Tu, H., Burke, T.M., Oderup, C., Huang, K., Wong, K., Lewén, S., LaJevic, M., and Zabel, B.A. (2014). Robust expansion of dendritic cells in vivo by hydrodynamic FLT3L-FC gene transfer. *J. Immunol. Methods* 413, 69–73.
 46. Yang, Y., Han, L., Yuan, Y., Li, J., Hei, N., and Liang, H. (2014). Gene co-expression network analysis reveals common system-level properties of prognostic genes across cancer types. *Nat. Commun.* 5, 3231.